




Energy exchange rate coefficients from vibrational inelastic $O_2(^3\Sigma_g^-) + O_2(^3\Sigma_g^-)$ collisions on a new spin-averaged potential energy surface

Cite as: J. Chem. Phys. 154, 064304 (2021); <https://doi.org/10.1063/5.0041244>

Submitted: 21 December 2020 . Accepted: 15 January 2021 . Published Online: 09 February 2021

 Qizhen Hong,  Quanhua Sun,  Fernando Pirani,  Mónica A. Valentín-Rodríguez,  Ramón Hernández-Lamonedá,  Cecilia Coletti,  Marta I. Hernández, and  Massimiliano Bartolomei



View Online



Export Citation



CrossMark



SHFQA
Quantum Analyzer
8.5GHz

Zurich Instruments

Your Qubits. Measured.

Meet the next generation of quantum analyzers

- Readout for up to 64 qubits
- Operation at up to 8.5 GHz, mixer-calibration-free
- Signal optimization with minimal latency

Find out more



Energy exchange rate coefficients from vibrational inelastic $O_2(^3\Sigma_g^-) + O_2(^3\Sigma_g^-)$ collisions on a new spin-averaged potential energy surface

Cite as: J. Chem. Phys. 154, 064304 (2021); doi: 10.1063/5.0041244

Submitted: 21 December 2020 • Accepted: 15 January 2021 •

Published Online: 9 February 2021



View Online



Export Citation



CrossMark

Qizhen Hong,^{1,2} Quanhua Sun,^{1,2} Fernando Pirani,³ Mónica A. Valentín-Rodríguez,⁴
Ramón Hernández-Lamoneda,⁴ Cecilia Coletti,^{5,a)} Marta I. Hernández,⁶
and Massimiliano Bartolomei⁶

AFFILIATIONS

¹State Key Laboratory of High Temperature Gas Dynamics, Institute of Mechanics, Chinese Academy of Sciences, 100190 Beijing, China

²School of Engineering Science, University of Chinese Academy of Sciences, Beijing 100049, China

³Dipartimento di Chimica, Biologia e Biotecnologie, Università di Perugia, via Elce di Sotto, 8 - 06183 Perugia, Italy

⁴Centro de Investigaciones Químicas-ICBA, Universidad Autónoma del Estado de Morelos, Cuernavaca 62210, Morelos, Mexico

⁵Dipartimento di Farmacia, Università G. d'Annunzio Chieti-Pescara, via dei Vestini, 66100 Chieti, Italy

⁶Instituto de Física Fundamental - CSIC, C/Serrano 123, Madrid, Spain

Note: This paper is part of the JCP Special Collection in Honor of Women in Chemical Physics and Physical Chemistry.

^{a)}Author to whom correspondence should be addressed: ccoletti@unich.it

ABSTRACT

A new spin-averaged potential energy surface (PES) for non-reactive $O_2(^3\Sigma_g^-) + O_2(^3\Sigma_g^-)$ collisions is presented. The potential is formulated analytically according to the nature of the principal interaction components, with the main van der Waals contribution described through the improved Lennard-Jones model. All the parameters involved in the formulation, having a physical meaning, have been modulated in restricted variation ranges, exploiting a combined analysis of experimental and *ab initio* reference data. The new PES is shown to be able to reproduce a wealth of different physical properties, ranging from the second virial coefficients to transport properties (shear viscosity and thermal conductivity) and rate coefficients for inelastic scattering collisions. Rate coefficients for the vibrational inelastic processes of O_2 , including both vibration-to-vibration (V-V) and vibration-to-translation/rotation (V-T/R) energy exchanges, were then calculated on this PES using a mixed quantum-classical method. The effective formulation of the potential and its combination with an efficient, yet accurate, nuclear dynamics treatment allowed for the determination of a large database of V-V and V-T/R energy transfer rate coefficients in a wide temperature range.

Published under license by AIP Publishing. <https://doi.org/10.1063/5.0041244>

I. INTRODUCTION

Molecular interactions involving oxygen molecules are of great relevance in atmospheric chemistry,¹⁻⁵ plasma physics,⁶⁻⁸ and hypersonic flow chemistry in atmospheric entries.⁹⁻¹³ In such situations, the population of vibrational states of oxygen molecules

usually strongly deviates from the Boltzmann distribution, showing a thermal nonequilibrium state. Moreover, the oxygen molecule will dissociate into oxygen atoms if the temperature is high enough; thus, the gas is also chemically not at equilibrium.

In order to describe gaseous systems in the above significant nonequilibrium state by numerical modeling, one should use the

state-to-state approach to trace the variation of internal energy levels and reproduce the evolutionary processes.^{14–16} The accuracy of the vibrational state-specific simulations, thus, relies on the accuracy of the rate coefficients of vibration–translation/rotation (V–T/R) and vibration–vibration (V–V) energy exchange processes, as well as of the rate coefficients for the dissociation involving the full ladder of vibrationally excited oxygen states (V–D). In such nonequilibrium conditions, highly excited vibrational states can largely contribute to dissociation and vibrational energy can, in turn, be removed by the reactive processes.

A lot of work has been devoted to provide kinetic data of reactions involving oxygen. For O₂–O collisions, Esposito *et al.* proposed a database, based on quasi classical trajectory (QCT) calculations, encompassing possible multi-quantum V–T/R relaxation rates and V–D dissociation coefficients for the overall manifold of vibrational levels of O₂.^{17,18} More recently, Andrienko pointed out the necessity to account for the complete ensemble of excited O₃ potential energy surfaces (PESs) when high temperature kinetics is of interest.¹⁹ For O₂–O₂ collisions, many investigations focused on the modeling of astrophysical environments and are, thus, often limited to the V–V relaxation of highly vibrational excited oxygen molecules at low temperatures ($T \leq 500$ K).^{4,20,21} A large dataset of V–T/R and V–V rates in a wide range of vibrational levels ($v \leq 29$) and a larger temperature range (up to 1000 K) was obtained by Coletti and Billing,²² using an analytical PES, whose parameters for the isotropic contribution were fitted by the absolute value of the experimental scattering cross sections,²³ but anisotropic contributions and spin–spin interactions were neglected. However, the high temperature and low pressure conditions characterizing, for instance, hypersonic flows around space flight vehicles (capsules reentered from the low Earth orbit or hypersonic cruisers) would require data at larger temperature to be considered.^{13,14} For this purpose, da Silva *et al.* used the forced harmonic oscillator (FHO) model to generate a multi-quantum dataset of V–T/R and V–D rates for O₂–O₂ collisions for a temperature up to 100 000 K.²⁴ In this approach, V–V transition processes were treated approximately to reduce the computational burden. However, as they pointed out, the results of the FHO model relying on a 1D Morse potential cannot be as accurate as the results of a method based on a full 3D potential. A larger dataset for vibration–vibration–translation transitions was more recently developed by Hao *et al.*¹⁴ in the 1000 K–20 000 K temperature range based on a similar FHO method. Such datasets, although covering a large temperature range and many vibrational states, cannot provide a benchmark set of state-specific vibrational relaxation rates,²⁴ more accurate PESs, and a more robust scattering method being needed for such a purpose.

Due to the importance of O₂–O₂ interactions, a number of *ab initio* potentials have been developed over the years. The accurate description of the electronic structure of the oxygen dimer is a challenging task: the complexity is due to the interaction of two open-shell molecules in the ${}^3\Sigma_g^-$ ground state, giving rise to singlet, triplet, and quintet PESs, which are degenerate at the asymptotic limit. Further complexity comes from the presence of two relatively low-lying electronically excited states of O₂, $a^1\Delta_g$ and $b^1\Sigma_g^+$.

Bartolomei *et al.* reported *ab initio* global PESs for the O₂(${}^3\Sigma_g^-$)–O₂(${}^3\Sigma_g^-$) dimer for all three spin states by combining restricted coupled cluster theory with complete active space second-order perturbation theory.^{25,26} Those PESs are four-dimensional

due to the rigid monomer assumption. Full six-dimensional PESs for singlet, triplet, and quintet spin coupling were later developed by Paukku *et al.*^{11,27} with the aim of studying high energy O₂(${}^3\Sigma_g^-$)–O₂(${}^3\Sigma_g^-$) collisions and including the possible reactive channels based on MS-CASPT2/maug-cc-pVTZ electronic structure calculations. Since their aim was an accurate description of the short range region (up to several hundred kcal/mol) for the modeling of high energy collisions and of reactivity, the corresponding *ab initio* points are mainly gathered at small intermolecular distances, and the long range region is comparatively very poorly sampled. This is bound to produce problems in the modeling of low energy collisions, although it is difficult to make a quantitative estimation for the reliable temperature range of these PESs. Recently, a direct molecular simulation was conducted using these potentials,²⁸ and vibrational relaxation time and dissociation rate coefficients were computed for O₂–O₂ collision at a temperature larger than 5000 K and were found to agree with the experimental data within the corresponding experimental uncertainty.

Moreover, a new global PES for the singlet spin state O₄ system was reported by Mankodi *et al.*¹² using the CASPT2/aug-cc-pVTZ level of theory and a novel point generation scheme, and the reported surface matches well with the singlet surface by Paukku *et al.*¹¹ Most recently, some of the authors reported high level unrestricted CCSD(T) *ab initio* data at the complete basis set limit for the intermolecular O₂(${}^3\Sigma_g^-$)–O₂(${}^3\Sigma_g^-$) potentials of the three spin multiplicities,²⁹ which represent an important benchmark for evaluating the correct behavior of the involved interaction.

In addition to the above available *ab initio* PESs, analytical potentials exploiting the partitioning of the interaction according to different contributions (exchange–repulsion, electrostatic, induction, and dispersion components) are often built in view of the calculation of kinetic data for a variety of processes. Bussery and Wormer³⁰ proposed van der Waals intermolecular potentials for rigid monomers (O₂)₂ in the three spin multiplicities. Aquilanti *et al.*²³ also reported PESs for rigid (O₂)₂ by expanding the interaction in spherical harmonics, separating the radial and the angular dependencies, and the parameters in the analytical formulation are tuned mostly on molecular beam scattering data.

We recently started a thorough investigation for the calculation of large datasets of rate coefficients for inelastic scattering, namely, vibration to vibration (V–V) and vibration to translation/rotation (V–T/R) energy transfer processes, in a series of diatom–diatom and atom–diatom systems. For such determination, the indispensable starting point is the accurate description of the potential, including the long and medium range regions, since inelastic scattering is very sensitive to long range effects (e.g., V–T/R coefficients need the initial separation distances between the colliding partners of several tens of Angstroms) and to the anisotropic component of the interaction. For this reason, analytical potentials are often found to provide a better choice than *ab initio*-based ones, which in some cases use a very limited number of points to describe the wide asymptotic interaction region. Although some neural network based methods, such as the recently developed permutation invariant polynomial-neural network approach,^{31–33} showed a good description of the long range as well as of the bound and repulsive regions, many interpolation procedures can introduce additional uncertainty to the accurate fitting of that part of the potential.

For the calculation of inelastic rate coefficients for $N_2 + N_2$ collisions in a wide temperature range (100 K–7000 K),³⁴ we recently used a formulation of the PES, representing the intermolecular potential in terms of an electrostatic and a van der Waals component, with the latter described according to the Improved Lennard-Jones (ILJ) model.³⁵ The corresponding parameters have a stringent physical meaning, as they account for the contribution to the van der Waals component of the interaction of different reciprocal orientations of the diatoms, and are fine-tuned against experimental or *ab initio* data. This makes it a powerful tool to get physical insights on the nature of the interaction, as well as on the understanding of the anisotropy and orientation effects that often determine the evolution of the collisional process.

We here apply the above procedure for the construction of a reliable potential for the non-reactive collisions of $O_2(^3\Sigma_g^-)$ molecules by considering a spin-averaged behavior, i.e., the employed parameters are chosen so to take into account for the statistical average over the singlet, triplet, and quintet low-lying PESs. In particular, while reactive events are driven by a specific spin state surface, the competition between inelastic and elastic processes is affected by collisions over all accessible PESs whose relative role and contribution are defined according to their spin multiplicity. Indeed, data from molecular beam experiments, probing large and intermediate intermolecular distances, have shown that for the three spin multiplicities, there are only small differences (compared to the extent of the van der Waals contribution) in the strength of the interaction whose global effect on the observables mostly depends on their average behavior.^{23,36} With respect to the formulation used for previous systems,^{34,35} we improved the flexibility of the PES by adding further angular dependence in some of the parameters.

On this new PES, we calculated a large database of V–V and V–T/R rate coefficients for a temperature up to 5000 K where vibrational transitions dominate. At higher temperature, the opening of the reactive channels cannot be neglected. The database includes vibrational excited states of molecular oxygen up to 30, which we consider the maximum confidence value related to the capability of the potential and of the Morse wavefunction in the nuclear dynamics treatment (see below) to represent molecular deformations.

As mentioned before, there are previous studies on vibrational relaxation of $O_2 + O_2$,^{4,20–22} but they are limited to lower temperature and restricted to fewer vibrational transitions. More recent and larger datasets^{14,24} are based on the approximate semiclassical FHO method, which, however, is known to lead to inaccuracies particularly when calculating resonant and quasiresonant transition rates at low temperature. In the present investigation, we use the more rigorous mixed quantum–classical method developed by Billing^{37–39} for the treatment of inelastic scattering, where vibrations are described in a quantum mechanical framework, whereas rotations and translation follow a classical description, and the coupling between the two sets of degrees of freedom is obtained through an Ehrenfest potential. Considering that for heavy nuclei translation and rotations behave mainly classically in the chosen temperature range, all the relevant quantum effects are appropriately considered for the inelastic scattering processes.

This paper is organized as follows. Sec. II is devoted to briefly describing the quantum–classical method. In Sec. III, the

formulation of the new spin-averaged $O_2(^3\Sigma_g^-)$ – $O_2(^3\Sigma_g^-)$ PES is given in detail; in the first part of Sec. IV, its performance is tested against a large number of different experimental measures, whereas the second part of Sec. IV describes the qualitative and quantitative features of the database obtained with the new PES. Concluding remarks are given in Sec. V.

II. THE QUANTUM–CLASSICAL METHOD

The quantum–classical method was introduced and developed by Billing^{37,38} and is proven to be an accurate and effective technique to obtain cross sections and rate coefficients for vibrational energy exchange processes involving heavy nuclei. The key feature of this method is that the vibrational degrees of freedom are treated quantum mechanically, whereas the other degrees of freedom (the translational and the rotational motion) are treated classically. In order to handle the whole system in a self-consistent way, the quantum mechanical degrees of freedom must evolve correctly under the influence of the surrounding classical motions. In turn, the classical degrees of freedom must respond correctly to quantum transitions.

According to the spirit of the quantum–classical method, vibration and roto-vibrational coupling are treated quantum mechanically by close coupled equations. Note that this formulation of the quantum–classical method is specifically designed to deal with non-reactive scattering processes. The total wavefunction is expanded in terms of the product of rotationally distorted Morse wavefunctions $\phi_{v_1}(r_1, t)\phi_{v_2}(r_2, t)$ as follows:

$$\Psi(r_1, r_2, t) = \sum_{v_1 v_2} a_{v_1 v_2}(t) \phi_{v_1}(r_1, t) \phi_{v_2}(r_2, t) \exp\left[-\frac{it(E_{v_1} + E_{v_2})}{\hbar}\right], \quad (1)$$

where r_i is the intramolecular distance of diatom i and E_{v_i} is the eigenvalue of the rotationally distorted Morse wave function $\phi_{v_i}(r_i, t)$ perturbed by roto-vibrational coupling,

$$\phi_{v_i}(r_i, t) = \phi_{v_i}^0(r_i) + \sum_{v'_i \neq v_i} \phi_{v'_i}^0(r_i) \frac{H_{v'_i v_i}}{E_{v_i}^0 - E_{v'_i}^0}, \quad (2)$$

where $H_{v'_i v_i}$ is the first-order centrifugal stretching term,

$$H_{v'_i v_i} = -j_i^2 m_i^{-1} \bar{r}_i^{-3} \langle \phi_{v'_i}^0 | r_i - \bar{r}_i | \phi_{v_i}^0 \rangle, \quad (3)$$

and j_i is the rotational momentum of molecule i , and the operator $\langle \rangle$ is obtained by integrating over r_i . $\phi_{v_i}^0$ is the unperturbed eigenfunction of the Morse oscillator, and $E_{v_i}^0$ is the eigenvalue approximated as

$$E_{v_i}^0 = \hbar\omega_e \left(v_i + \frac{1}{2}\right) - \hbar\omega_e x_e \left(v_i + \frac{1}{2}\right)^2 + \hbar\omega_e y_e \left(v_i + \frac{1}{2}\right)^3, \quad (4)$$

where ω_e is the oscillator wavenumber and x_e and y_e are the anharmonicity constants (Table I).

TABLE I. Molecular constants for $O_2(^3\Sigma_g^-)$.⁴⁵

ω_e	1580.3 cm^{-1}
x_e	0.007 639
y_e	0.000 0345
r_e	1.207 Å
β_e	2.532 Å ⁻¹
D_e	5.215 eV
Q_e	-0.239 a.u.

In order to obtain the amplitudes $a_{v_1'v_2'}$ for the inelastic processes $O_2(v_1) + O_2(v_2) \rightarrow O_2(v_1') + O_2(v_2')$, one can, thus, plug expansion (1) into the time-dependent Schrödinger equation and obtain the following set of coupled equations for the amplitudes:

$$i\hbar\dot{a}_{v_1'v_2'}(t) = \sum_{v_1v_2} \left[\left\langle \phi_{v_1'}^0 \phi_{v_2'}^0 \right| V(r_1, r_2, t) + \sum_k 2i\hbar j_k \frac{dj_k}{dt} \right. \\ \left. \times \frac{\langle \phi_{v_1'}^0 | (r_k - \bar{r}_k) | \phi_{v_1}^0 \rangle \langle \phi_{v_2'}^0 | \phi_{v_2}^0 \rangle}{m_k r_{eq,k}^3 (E_{v_1}^0 - E_{v_1'}^0)} \right] \\ \times a_{v_1v_2}(t) \exp \left[\frac{i}{\hbar} (E_{v_1'} + E_{v_2'} - E_{v_1} - E_{v_2}) t \right]. \quad (5)$$

The translational and rotational motions are obtained by solving the corresponding Hamilton equations by making use of an Ehrenfest averaged potential⁴⁰ defined as the quantum expectation value of the interaction potential. This mean-field method usually provides accurate quantum transition probabilities and properly conserves total (quantum plus classical) energy. A variable-order variable-step Adams predictor-corrector integrator⁴¹ is then used to solve the coupled equations [Eq. (5)] and the classical equations of motion for rotations and translation. An absolute integration accuracy of 10^{-8} is achieved for all calculations in this work.

The vibrational wavefunction is initialized as the product of the Morse wavefunctions for the two infinitely separated diatoms. The simultaneous propagation of the quantum and classical sets of equations produces the quantum transition amplitudes $a_{v_1'v_2'}$, which can be used to calculate cross sections for the vibrational transitions. The cross sections are obtained by averaging over a number of trajectories having randomly selected initial conditions, and a Monte Carlo average over the initial Boltzmann distribution of rotational energy is generally introduced to have rate coefficients for vibrational relaxation. Thus, an average cross section is defined as

$$\sigma_{v_1v_2 \rightarrow v_1'v_2'}(T_0, \bar{U}) = \frac{\pi\hbar^6}{8\mu k_B^3 T_0^3 I_1 I_2} \int_0^{l_{\max}} \int_0^{j_1 \max} \int_0^{j_2 \max} dj_1 dj_2 dl \\ \times (2j_1 + 1)(2j_2 + 1)(2l + 1) |a_{v_1'v_2'}|^2, \quad (6)$$

where μ is the reduced mass for the relative motion of the diatoms and l is the orbital angular momentum. The moment of inertia is $I_i = m_i r_i^2$, and the temperature T_0 is arbitrary because it cancels when calculating the rate coefficients. $j_1 \max$ and $j_2 \max$ are the upper limits for the randomly chosen rotational quantum numbers for the diatoms, and l_{\max} is the upper limit for the angular momentum. Rate coefficients are then calculated through the following equation:

$$k_{v_1v_2 \rightarrow v_1'v_2'}(T) = \left(\frac{8k_B T}{\pi\mu} \right)^{1/2} \left(\frac{T_0}{T} \right)^3 \int_0^\infty d \left(\frac{\bar{U}}{k_B T} \right) \\ \times \exp \left(-\frac{\bar{U}}{k_B T} \right) \sigma_{v_1v_2 \rightarrow v_1'v_2'}(T_0, \bar{U}), \quad (7)$$

which holds for exothermic processes. \bar{U} , the symmetrized classical energy, is introduced to restore the detailed balance principle.^{37,40}

Transport properties (such as shear viscosity and thermal conductivity) for diatomic gases can also be calculated through the present quantum-classical method,⁴² combining it with the first-order Sonine expansion of the Wang Chang-Uhlenbeck theory.⁴³ Specifically, the shear viscosity η and thermal conductivity λ are defined, respectively, as

$$\eta^{-1} = \frac{8}{5k_B T} \left\{ \left\{ \gamma^4 \sin^2 \xi - \frac{1}{2} (\Delta\epsilon)^2 \sin^2 \xi + \frac{1}{3} (\Delta\epsilon)^2 \right\} \right\} \quad (8)$$

and

$$\lambda = \frac{\eta k_B}{m} \left[\frac{15}{4} + \beta_T c_{\text{int}}' - \frac{2c_{\text{int}}(5/2 - \beta)}{\pi\rho + 2(5/2c_{\text{int}}' + \beta)} \right], \quad (9)$$

where

$$\beta_T = \frac{3c_{\text{int}} T}{8\eta} \left\{ \left\{ (\epsilon_i - \bar{\epsilon}) [(\epsilon_i - \epsilon_j) \gamma^2 - (\epsilon_k - \epsilon_j) \gamma \gamma' \cos \xi] \right\} \right\}^{-1}, \quad (10)$$

where $\epsilon_i = E_i/k_B T$, ξ is the scattering angle, $\gamma^2 = mv^2/4k_B T$, and c_{int} is the internal heat capacity. Further details can be found in Ref. 42. A Monte Carlo procedure is used to average over the molecular collisions, computed by the present quantum-classical method, in order to obtain the collision integrals $\langle \{ \} \rangle$, which can be written as

$$\langle \{ \} \rangle = \int_0^\infty d \left(\frac{\bar{U}}{k_B T} \right) \sigma_{\{ \}}(\bar{U}) \exp \left(-\frac{\bar{U}}{k_B T} \right), \quad (11)$$

with

$$\sigma_{\{ \}}(\bar{U}) = \frac{\pi\hbar^6}{8\mu k_B^3 T^3 I_1 I_2} \left(\frac{8k_B T}{\pi\mu} \right)^{1/2} \int_0^{l_{\max}} \int_0^{j_1 \max} \int_0^{j_2 \max} dj_1 dj_2 dl \\ \times (2j_1 + 1)(2j_2 + 1)(2l + 1) \frac{\{ \}}{N}, \quad (12)$$

in which N is the number of trajectories calculated at a given value of the symmetrized classical energy.

III. POTENTIAL ENERGY SURFACE

The construction of the present spin-averaged (i.e., representing an average behavior of the singlet, triplet, and quintet PESs) PES essentially relies on the same basic ingredients of those developed in Refs. 34, 35, and 44, where the idea of an Improved Lennard-Jones (ILJ) description for atom–molecule and molecule–molecule interactions has provided a reliable and accurate determination of the intermolecular potential of weakly interacting systems.

In this study, combined with the angular dependence of size (exchange) repulsion and dispersion attraction, we introduce additional flexibility to the interaction potential formulation by modulating its shape, or the reduced form, according to the relative orientation of the colliding diatoms. This further improvement has been suggested by an internally consistent analysis of the large variety of experimental data taken into account, as will be shown in Sec. IV.

As in the previous formulations, we express the overall interaction V of the diatom–diatom system as a sum of intramolecular (V_{intra}) and intermolecular (V_{inter}) interaction components. Specifically, V_{intra} is formulated using a Morse potential energy function $D_e(t^2 - 2t)$, in which D_e is the dissociation energy of the diatomic molecule, $t = \exp[-\beta(r - r_e)]$, and r is the bond length of the molecule (with r_e being its equilibrium value). The Morse parameters employed in the present calculations are listed in Table I and are also used to define the Morse wavefunction for the quantum-classical calculation.

The intermolecular (V_{inter}) interaction component is represented in terms of two main contributions,

$$V_{inter} = V_{vdW} + V_{elect}, \quad (13)$$

where the V_{vdW} term accounts indirectly for three body effects, being formulated as a combination of bond–bond pair contributions.^{35,44} Indeed, zero order parameters are obtained by the tensor components of molecular bond polarizabilities, and they have been fine-tuned during the combined analysis of theoretical and experimental data discussed in the following. The V_{elect} term defines the electrostatic interaction due to the molecular permanent multipoles: only the main quadrupole–quadrupole term is retained in the case of interaction between homonuclear molecules.^{34,35}

Generally, the V_{vdW} interaction (size repulsion plus dispersion attraction) depends not only on the distance R between the centers of mass of the interacting partners but also on θ_a, θ_b, Φ , the four body Jacobi angular coordinates, which describe the relative orientation of the two diatoms. Specifically, the V_{vdW} component is expressed as an improved Lennard-Jones (ILJ) potential as follows:^{44,46}

$$V_{vdW}(R, \gamma) = \varepsilon(\gamma) \frac{6}{n(R, \gamma) - 6} \left(\frac{R_m(\gamma)}{R} \right)^{n(R, \gamma)} - \varepsilon(\gamma) \frac{n(R, \gamma)}{n(R, \gamma) - 6} \left(\frac{R_m(\gamma)}{R} \right)^6, \quad (14)$$

where $\gamma = (\theta_a, \theta_b, \Phi)$ and ε and R_m are the bond–bond interaction well depth and its location, respectively. This function gives a more

realistic representation of both the repulsion and the long range attraction than the classic Lennard-Jones potential.⁴⁷ The n term is expressed as a function of both R and γ ,

$$n(R, \gamma) = \beta(\gamma) + 4.0 \left(\frac{R}{R_m(\gamma)} \right)^2. \quad (15)$$

At variance with previous derivations,^{34,35} in this case, $\beta(\gamma)$, a parameter related to the hardness of the interacting partners, is no longer fixed to a constant value but considered depending on the reciprocal orientation of the diatoms. This flexibility allows us to vary the shape of the potential as a function of the configuration assumed by the system.

The angular dependence of the V_{vdW} term is obtained by representing the potential parameters ε , R_m and β in a spherical harmonic expansion. Thus, the reduced form of the V_{vdW} component is considered to be the same for all orientations, as stressed in Refs. 35 and 48. It is sufficient to truncate the expansion to the fifth term so to have the following:³⁵

$$\varepsilon(\gamma) = \varepsilon^{000} + \varepsilon^{202} A^{202}(\gamma) + \varepsilon^{022} A^{022}(\gamma) + \varepsilon^{220} A^{220}(\gamma) + \varepsilon^{222} A^{222}(\gamma), \quad (16)$$

$$R_m(\gamma) = R_m^{000} + R_m^{202} A^{202}(\gamma) + R_m^{022} A^{022}(\gamma) + R_m^{220} A^{220}(\gamma) + R_m^{222} A^{222}(\gamma), \quad (17)$$

$$\beta(\gamma) = \beta^{000} + \beta^{202} A^{202}(\gamma) + \beta^{022} A^{022}(\gamma) + \beta^{220} A^{220}(\gamma) + \beta^{222} A^{222}(\gamma), \quad (18)$$

where the coefficients $\varepsilon^{L_1 L_2 L}$, $R_m^{L_1 L_2 L}$ and the bipolar spherical harmonics $A^{L_1 L_2 L}$ can be obtained as described in Ref. 35, and we only give here the explicit expressions for $\beta^{L_1 L_2 L}$,

$$\begin{aligned} \beta^{000} &= \frac{1}{9} (2\beta^H + 2\beta^X + 2\beta^{T_a} + 2\beta^{T_b} + \beta^L), \\ \beta^{202} &= \frac{2}{9\sqrt{5}} (-\beta^H - \beta^X - \beta^{T_a} + 2\beta^{T_b} + \beta^L), \\ \beta^{022} &= \frac{2}{9\sqrt{5}} (-\beta^H - \beta^X + 2\beta^{T_a} - \beta^{T_b} + \beta^L), \\ \beta^{220} &= \frac{2}{9\sqrt{5}} (2\beta^H - \beta^X - \beta^{T_a} - \beta^{T_b} + \beta^L), \\ \beta^{222} &= \frac{\sqrt{14}}{45} (\beta^H - 2\beta^X + \beta^{T_a} + \beta^{T_b} - \beta^L). \end{aligned} \quad (19)$$

The values of the parameter β for the relevant configurations, H (parallel), L (linear), T (T-shaped), and X (crossed), are listed in Table II, together with the corresponding ones for ε and R_m .

The V_{elect} term of Eq. (13) is given by

$$V_{elect}(R, \gamma) = \frac{Q_a Q_b}{R^5} A^{224}(\gamma), \quad (20)$$

TABLE II. Parameters for the O₂–O₂ intermolecular potential. R_m (Å), ϵ (meV), and β values define the vdW components in the relevant configurations of the complexes, given by the θ_a , θ_b , and Φ angles (in degrees), corresponding to the monomers at the equilibrium bond length, r_e .

Configuration, i	$(\theta_a, \theta_b, \Phi)$	R_m^i	ϵ^i	β^i
H	(90,90,0)	3.56	15.21	9
X	(90,90,90)	3.56	15.21	9
T _a = T _b	(90,0,0)	3.97	10.40	10
L	(0,0,0)	4.41	8.88	11.2

where Q_a and Q_b (the value at equilibrium bond length Q_e is reported in Table I) correspond to the quadrupole moments of the monomers⁴⁹ and $A^{224}(\gamma)$ is the bipolar spherical harmonic, which describes the angular dependence of the quadrupole–quadrupole interaction.

The above formulas are completely general, and each term in the expression is physically meaningful.

Note that both V_{vdW} and V_{elect} intermolecular components include the dependence on monomer deformations by exploiting the bond length dependence of O₂ polarizability and quadrupole moment, which has been previously reported in Ref. 50 (see Figs. 5 and 6 as well as the Appendix therein). The same approach has been previously and successfully used to describe the global interaction in the O₂–N₂⁵⁰ and N₂–N₂³⁴ dimers, and we consider that the proposed formulation is reliable for monomer deformations up to 40%, a requirement that allows us to represent the behavior of vibrationally excited molecules for ν up to 20–25.

Moreover, *ab initio* calculations of the O₂–O₂ interaction with stretched monomers show that the trends of the related potential energy curves, corresponding to the dimer limiting configurations, are consistent with those provided by the present semiempirical formulation (see, for example, Fig. S1 of the supplementary material for a comparison related to the L configuration with monomers stretched of 10% with respect to equilibrium distance).

The three spin multiplicity supermolecular *ab initio* interaction energies of O₂(³Σ_g[−])–O₂(³Σ_g[−]) for some selected basic configurations, which are those describing the main features of the global potential (H, L, T, and X), have been recently computed²⁹ at the UCCSD(T) level of theory using augmented correlation consistent basis sets⁵¹ up to the complete basis set extrapolation.⁵² Those high accuracy data can be used to obtain spin-averaged *ab initio* energies and are, thus, valuable for assessing the present PES.

The comparison of the present PES with such *ab initio* data and with existing semiempirical PESs, some of them built by using the same set of experimental molecular beam scattering data of Ref. 23, is reported in Fig. 1, which depicts the potential energy as a function of the intermolecular distance R of the diatoms at their equilibrium geometry for the reference configurations.

In particular, Fig. 1 includes the spin-averaged rigid monomer PES of Aquilanti *et al.*,²³ which was fitted to molecular beam scattering data, and the Coletti and Billing analytical PES, where the dependence on r_1 and r_2 was explicitly included in the intermolecular potential and on which a dataset of quantum–classical V–V and V–T/R rates was constructed.²²

The comparison with the *ab initio* points (also reported in more detail in Fig. S2 of the supplementary material) shows that the present spin-averaged PES gives an excellent description of the long range and short range regions for all the investigated geometries, and the interaction potential well is in very good agreement for the X and L configurations, while some discrepancies appear for the T and H configurations. Since the nature of the formulation of the present spin-averaged PES allows us to investigate the contributions coming from different interaction regions or from different configurations, it would obviously be possible to change some of the parameters just to fit the *ab initio* points. However, the rationale behind the construction of this kind of potential energy surface is to have parameters that are numerically determined by their physical meaning and not by mechanical fitting procedures. A key feature in such an approach is, thus, the validation and, in case, the fine tuning of the PES against multiple properties (mainly experimental data of different origins, as will be shown in Sec. IV), with *ab initio* points being just one among them.

Although the present PES and those of Refs. 22 and 23 share the fact that they rely, even if to a different extent, on the same experimental dataset, their behavior, as their analytical functional form, is quite different. They are rather similar in the collinear configuration: the position of the well is nearly the same as for the *ab initio* points, with the Coletti–Billing PES showing the earliest and less deep well. In all the other configurations, the well position of the present PES is very close to the *ab initio* points, as is the Coletti–Billing one, but the latter tends to have deeper wells. The Aquilanti PES, on the contrary, although agreeing with the *ab initio* points for the T configuration, presents early wells for the H and X geometries.

Among those PESs, the newly introduced one, thus, presents the overall best behavior in the comparison with the *ab initio* points.

Figure 1 also shows the behavior of the recent reactive *ab initio* PES of Ref. 11 (indicated as UMN PES), which has been opportunely spin-averaged according to the different statistical populations of the spin multiplicities. Although this PES reasonably describes the short range regions for all geometries, its ability to represent the interaction minima and long range asymptotic behavior is very different according to the selected configuration. The depth of the collinear configuration well is quite in agreement with the *ab initio* results (better than the PESs described above) although it is less wide and is shifted at shorter interaction distances R . The PES fails to describe the interaction wells of the H and X configurations as it only presents a shallow variation with R in the long–medium range regions. In the T configuration, the well is again less wide and less deep with respect to the *ab initio* data. This seems to be an indication that the use of this kind of PES is probably advisable only at high temperature regimes, which are mainly driven by the short range part of the potential. One of the possible reasons of the low accuracy in the description of large interaction distances could be connected to the fact that the *ab initio* points used to build the PES, which is mostly focused on the description of reactive collisions,¹¹ are more concentrated in the short range regions (where reaction channels might open as well), whereas those in the medium–long range regions are sparse so that the interpolation procedure can easily produce large numerical errors or introduce spurious features.

Section IV shows that properties calculated with the PES introduced in the present investigation are in very good agreement

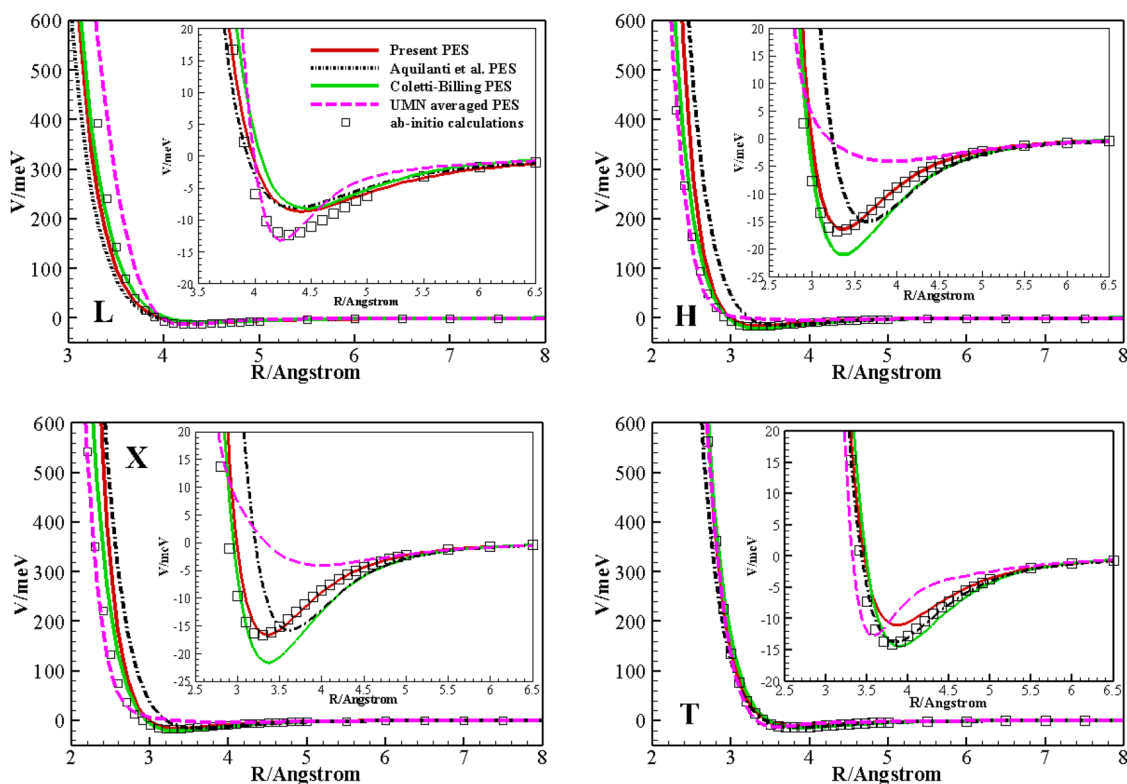


FIG. 1. Behavior of different PESs as a function of the intermolecular distance. Selected configurations, at the equilibrium intramolecular distance of both monomers, are considered: diatoms approaching according to a linear configuration L ($D_{\infty h}$ symmetry, panel L) in a parallel fashion (H configuration, D_{2h} symmetry, panel H); in a crossed X fashion (D_{2d} symmetry, panel X) and perpendicularly, according to a T orientation (C_{2v} symmetry, panel T).

with a wealth of experimental data of different kinds, thus ensuring a reliable basis to calculate, in the appropriate validity range, a large database of rate coefficients for scattering processes involving vibrational energy exchange.

IV. RESULTS AND DISCUSSION

A. Validation of the PES against experimental data

The description of various physical phenomena requires a potential energy surface correctly describing, for all possible configurations, large diatom–diatom interaction distances (up to several tens of Angstroms), the potential wells, and the first repulsive walls. The non-negligible effects often arise from the interplay of the different contributions to the full interaction potential and make it complicated to propose a potential suitable for all ranges. Because of this, we tested the ability of the present spin-averaged potential to reproduce the experimental data of different origins or sensitive to different regions of the potential, namely, experimental integral cross sections, second virial coefficients, transport properties, and V–T/R and V–V inelastic rates. The outcome of the latter is particularly meaningful for the subsequent part of the present work, i.e., the

determination of a large database of accurate V–V and V–T/R rate coefficients.

A first comparison can be made with total scattering cross sections measured through rotationally hot molecular beams.²³ The average component of the cross sections is connected to the average attraction at a long range, with the position and frequency of the *glory* oscillations directly related to the well features of the isotropic component of the interaction. Figure 2 depicts the spherical average of the potential calculated with the present PES and those already examined in Sec. III. The comparison shows that all the PESs based on the scattering data indeed present approximately the same behavior, which is also shared by the *ab initio* data. In particular, related well depth, minimum location, and the negative area of the potentials, determining frequency and extremum position of the quantum *glory* interference, resolved as an oscillating pattern in measurements of the velocity dependence of integral cross sections, appear to be very close. Moreover, the present PES provides a strength of the attraction at 6.5 Å, the distance mainly probed by the absolute value of the smooth component of measured cross sections,²³ of about -0.62 meV, which is in the range of experimental determination of about -0.70 ± 0.07 meV and of the combination of theoretical dispersion contributions, leading to -0.59 meV.⁴⁹ The spherical average of the potential calculated on the UMN PES, on

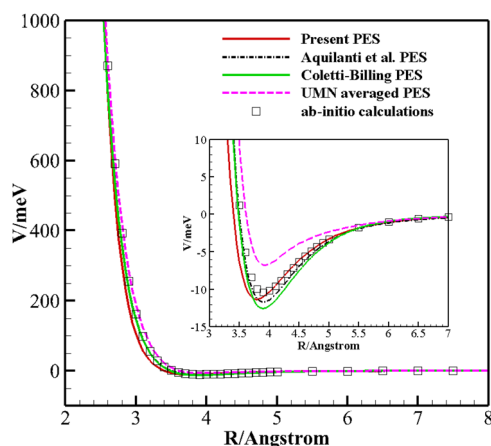


FIG. 2. Spherical average of different PESs as a function of the diatomic interaction distance.

the other hand, is less attractive and shows a less deep well, even if the minimum position is in agreement with the *ab initio* data and the other PESs.

The asymptotic C_6 dispersion coefficient predicted by the present PES amounts to $33.6 \text{ eV } \text{\AA}^6$, also in substantial agreement with the theoretical result of $37.2 \text{ eV } \text{\AA}^6$ of Ref. 49.

The second virial coefficient, $B(T)$, is another important benchmark for the quality of the potential: the negative values at low temperature are sensitive to the anisotropy of the attractive interaction, whereas the positive values at higher temperature are a probe of the first repulsive region. Thus, second virial coefficients $B(T)$, including the first quantum correction $B_{q1}(T)$ to the classical estimate $B_{c1}(T)$ ⁵³ [$B(T) = B_{q1}(T) + B_{c1}(T)$], have been calculated on the present PES. The comparison with the experimental measurements^{54,55} is reported in Table III where excellent agreement is found at low and medium temperatures ($T < 400 \text{ K}$), with calculated values lying well within the experimental bars. At higher temperature, the discrepancy is a little larger, but in any case, it amounts to 10% of the experimental value at most, which demonstrates that the present PES can accurately describe the medium and long range regions of the interaction.

Yet, another comparison can be made between experimental transport properties and those calculated by means of the present PES; such properties are indeed sensitive to the strength and anisotropy of the interaction in the first repulsion region of the potential. Shear viscosity and thermal conductivity of molecular oxygen were calculated as a function of temperature by using quantum classical cross sections computed on the newly introduced potential and on the other PESs shown in Fig. 1. For these calculations, both O_2 molecules were considered in the initial ground vibrational state, and cross sections were computed at the 47 initial values of total classical energy comprised between 35 cm^{-1} and $80\,000 \text{ cm}^{-1}$, with a more frequent sampling directed toward lower energies. For each energy value, 2000 trajectories were used, with an initial separation of the diatoms equal to 15 \AA , and an impact parameter randomly chosen between 0 \AA and 9 \AA , a value

TABLE III. Calculated and experimental second virial coefficient $B(T)$ given in cm^3/mol as a function of temperature.

T (K)	Present PES	Experiment ^{54,55}
90	-238.9	-241 ± 10
100	-195.6	-197 ± 7
140	-104.6	-104 ± 5
170	-72.0	-69 ± 4
210	-46.2	-45 ± 2
220	-41.6	-40 ± 2
250	-30.3	-29 ± 2
310	-15.3	-14 ± 1
380	-4.6	-3 ± 1
400	-2.4	-1 ± 1
406	-1.7	0 ± 1
600	10.9	13 ± 1
800	16.7	19 ± 1
1000	19.9	22.4 ± 1
1400	22.9	25.9 ± 1

ensuring that all the trajectories that might affect the desired properties are taken into account in the calculation.

As shown in the left panel of Fig. 3, the calculated shear viscosity coefficients are in excellent agreement with the experimental data⁵⁶⁻⁵⁸ in the whole temperature range considered here. All the other potentials also show satisfactory agreement at low temperature, but at higher T values, they tend to underestimate the experimental behavior (see Table S1 of the supplementary material). The comparison for thermal conductivity (Fig. 3, right panel and Table S2 of the supplementary material) is less stringent because the calculated values might be more sensitive to the neglect of higher order terms in the Wang Chang-Uhlenbeck theory. In this case, excellent agreement is still found at low temperature, whereas at high T , the present PES overestimates (by 10% at most) the experimental values. The other PESs, with the exception of the UMN one that matches the experimental data very well at high temperature, also tend to overestimate experimental values, although to a lower extent.

In view of the determination of the dataset of rate coefficients, we also tested the new PES for the calculation of V-V and V-T/R rates, comparing them to experimental data and to previous computational results available in the literature, over a wide range of temperatures. For a temperature higher than 5000 K , the opening of the reaction channels occurs and neither the present PES nor the quantum classical method employed here is able to properly take that into account. The details of the quantum classical calculations are the same as those for the determination of transport properties, with the obvious exception of the initial vibrational states of the diatoms. Moreover, an initial separation of the diatoms equal to 80 \AA (instead of 15 \AA) was used for V-T/R energy transfer, a larger value being needed to avoid the quenching of long range forces due to too close collisions.⁶⁰

The number of coupled vibrational states included in the set of the time-dependent quantum equations varies because of the closer

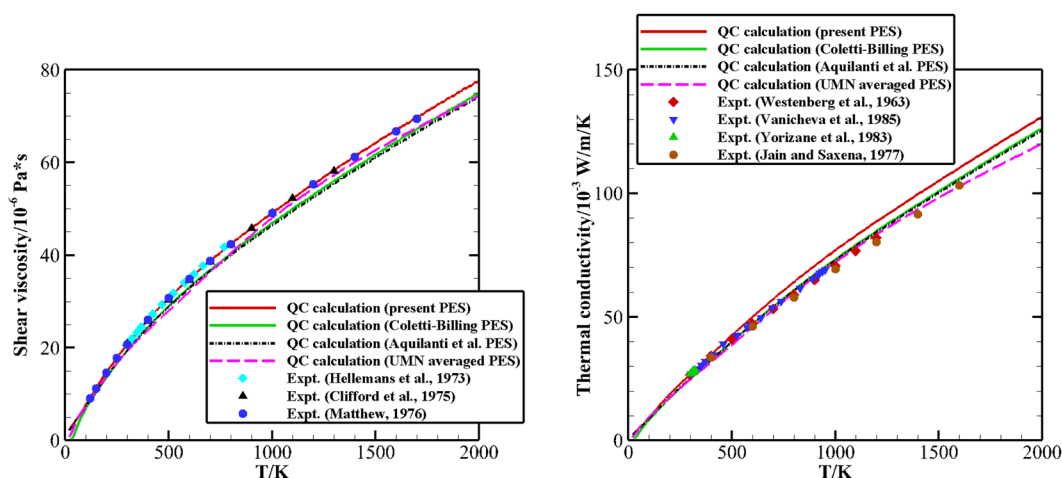


FIG. 3. Transport coefficients: shear viscosity (left panel) and thermal conductivity (right panel) of oxygen as a function of temperature. The red solid line shows the calculations based on the present PES, the green solid line shows the calculations based on the PES of Ref. 22, the black dotted line shows the calculations based on that of Ref. 23, and the pink dashed line shows the calculations based on that of Ref. 11. The quantum classical method described here was used in all cases. Experimental data of Refs. 56–58 are also reported.

vibrational spacing between levels at high v . We, thus, used 36 states for $v < 10$, 49 states for $10 \leq v < 20$, and 81 states for $20 \leq v \leq 30$.

Experimental data are available for the V–T/R process: $O_2(1) + O_2(0) \rightarrow O_2(0) + O_2(0)$ [hereafter indicated as (1,0) \rightarrow (0,0) in short], as well as for the following V–V processes: $O_2(v) + O_2(0) \rightarrow O_2(v-1) + O_2(1)$ [hereafter indicated as (v,0) \rightarrow (v-1,1) in short], and total relaxation rate coefficients (i.e., the sum of the rates for V–V and V–T/R processes) at 300 K and 465 K.

The V–T/R rates for the (1,0) \rightarrow (0,0) process calculated with the aforementioned PESs are reported in Fig. 4 and their numerical values in Table S3. The present spin-averaged PES results (red solid line) are in very good agreement with the experimental data of Ref. 59 at low temperature, and agreement remains

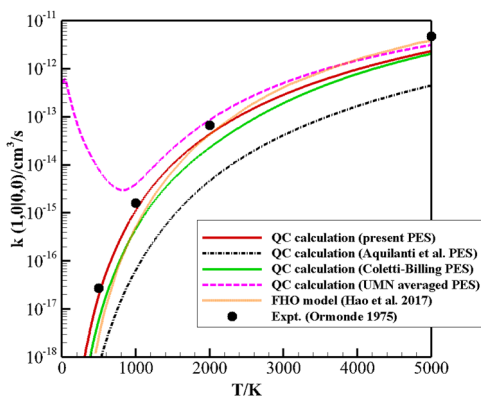


FIG. 4. Rate coefficients for the transition (1, 0) \rightarrow (0, 0) as a function of temperature calculated on the present PES (full red line) and on the available PESs. Experimental data of Ref. 59 (black circles) are also reported.

reasonably good, although they are lower than the experiments, at high temperature. Such an underestimation is more evident for the Coletti and Billing results in the whole temperature range, and the discrepancy is much more striking by the values predicted by using the PES of Aquilanti *et al.* (black dashed-dotted line), consequence of the rigid rotors' assumption. The UMN-averaged PES, on the contrary, presents good agreement with the experimental values at high temperature, while the predicted values have the wrong qualitative behavior in the low temperature regime, confirming the good representation of the potential at a short range (largely prevailing at high T) and a poor one for the long range region.

We also included in Fig. 4 the rate coefficients obtained by using the semiclassical Forced Harmonic Oscillator (FHO) model of Ref. 14, which show good agreement with the experimental data at $T \geq 2000$ K but a significant deviation at temperatures lower than 1000 K.

Figure 5 shows the V–V rate coefficients for the processes (v,0) \rightarrow (v-1,1) calculated with the present PES at 300 K, as well as calculations by Hernández *et al.*⁴ with the Vibrational Close Coupling - Infinite Order Sudden (VCC-IOS) method and by Coletti and Billing²² with the same quantum classical method employed here, and the experimental data.^{3,61–64} The measured values are available up to $v = 13$ and seem to point out that the V–V contribution is predominant for small v values, slightly increasing with v up to $v \approx 4$ while decreasing rapidly as v further grows. The rates calculated on the present PES (black solid line) agree well with the results of Ref. 61 (red diamonds in Fig. 5) for low values of v (see also Table S4), where, however, the experimental data obtained from different sources fall in a rather wide interval. For $v \geq 4$, the match with all experimental determinations is quite satisfactory and in line with those computed with the VCC-IOS method (also available starting from $v \geq 5$). A larger difference is instead found for the rate coefficients obtained in Ref. 22, where a less sharp decrease in the rates with v is predicted.

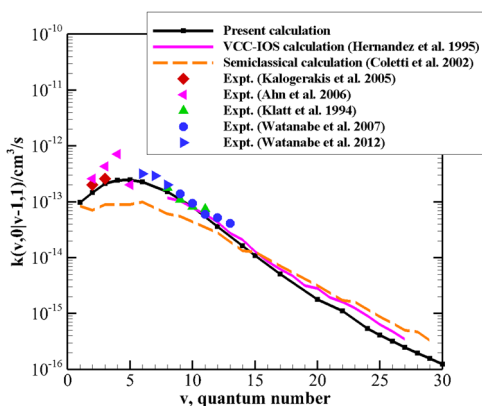


FIG. 5. Rate coefficients as a function of vibrational level for the $(v, 0) \rightarrow (v-1, 1)$ transition calculated on the present PES (black solid line with squares). The available calculations (pink solid line—Hernández *et al.*⁴ and orange dashed line—Coletti and Billing²²) and experimental data of Ref. 61 (red diamonds), Ref. 62 (pink left-triangles), Ref. 3 (green triangles), Ref. 63 (blue circles), and Ref. 64 (blue right-triangles) are also reported.

Figure 6 shows total vibrational relaxation rates ($k_{v,v-1}^{0,0} + k_{v,v-1}^{0,1}$) as a function of the initial vibrational level v at $T = 300$ K (Table S5) and 465 K (Table S6), left and right panels, respectively, available from experimental data^{1,3,65,66} and from previous theoretical determinations. The new PES provides the correct qualitative behavior of the relaxation rates as v increases, including the two inversions, related to the prevalence of V–V energy transfer at low v values (showing a peak in the relaxation efficiency at $v \approx 5$, as in Fig. 5), whereas V–T/R processes strongly increase with

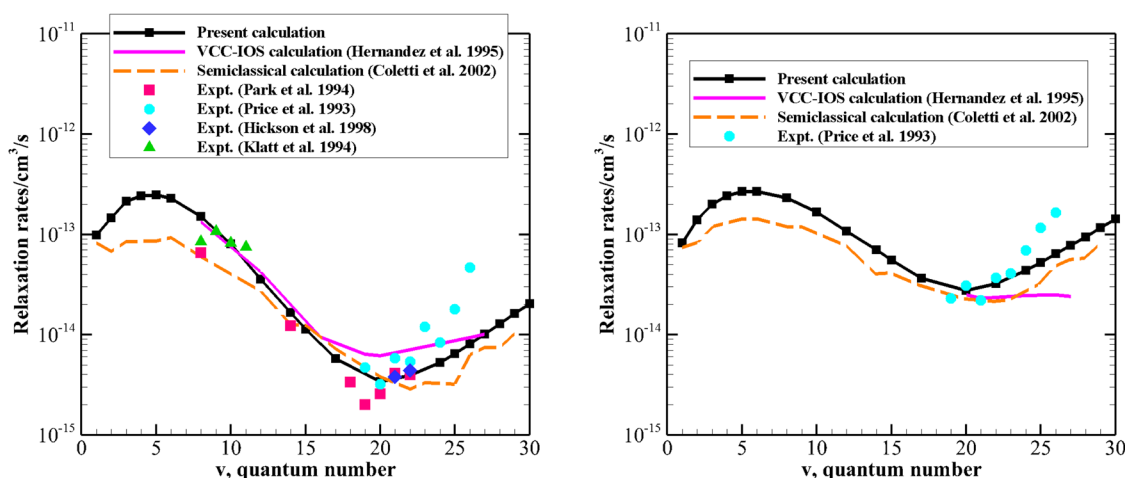


FIG. 6. Total vibrational relaxation rate coefficients as a function of vibrational level at $T = 300$ K (left panel) and at $T = 465$ K (right panel) calculated on the present PES (black solid line with squares). The available calculations (pink solid line—Hernández *et al.*⁴ and orange dashed line—Coletti and Billing²²) and experimental data of Ref. 1 (red squares), Ref. 65 (light blue circles), Ref. 66 (blue diamonds), and Ref. 3 (green left-triangles) are also reported.

v (see also Sec. IV B), becoming the predominant process at high v values ($v \geq 20$). The relaxation rates calculated over the present PES match quantitatively very well with experimental data for $v \leq 23$ at both temperatures. The results obtained in Ref. 22 also show the correct qualitative behavior, although the quantitative matching is liable to large statistical fluctuations, which, together with the worse matching of V–V coefficients of Fig. 5, suggests a too small number of trajectories employed in the quantum classical method and the use of the less accurate PES than the present one. The VCC-IOS results⁴ agree with the experimental data at v values around 20, but the inversion behavior in the rates is much less evident. All the calculated rates tend to underestimate the strong enhancement observed for $v > 23$ measured by Price *et al.*⁶⁵ Although a relatively lower accuracy in both the PES and the quantum classical methods might arise at the highest v values considered here, this behavior indicates that a different mechanism of energy transfer contributes to the overall vibrational relaxation at high v values.

Three possible mechanisms were mentioned in Ref. 4 to account for the discrepancy. First, the reactive channel leading to ozone formation opens for $v > 25$, and its coincidence with the sharp jump in rates is suggestive of its presence. Additionally, it is well known that the saddle-point region of the PES can lead to enhancement of the vibrational relaxation rates even if the reaction channel is closed. Finally, the presence of low-lying excited electronic states of O_2 ($a^1\Delta_g$ and $b^1\Sigma_g^+$) suggests that vibrational to electronic energy transfer could also be responsible. A reduced dimensionality quantum reactive scattering study⁶⁷ showed that the rates of the chemical reaction are too low to explain the observed enhancement, and a subsequent investigation²¹ of vibrational relaxation using a potential energy surface including the reactive channel clearly showed a marked enhancement of the rates for the higher vibrational levels, but this mechanism only partially accounted for the experimental observations. An important experimental breakthrough occurred

when a local perturbation of the $O_2(X^3\Sigma_g^-, \nu = 28)$ state with $O_2(b^1\Sigma_g^+, \nu = 19)$ due to spin-orbit coupling was spectroscopically determined.⁶⁸ The vibrational relaxation of $\nu = 28, 30$ was, then, studied⁶⁹ to further characterize the *dark-channel*, concluding on the relevance of V-E energy transfer and large multi-quantum transitions ($\Delta\nu = 9$). A series of theoretical studies⁷⁰⁻⁷² was performed in order to quantify the relevance of the V-E mechanism due to spin-orbit coupling, clearly indicating its importance in the observed jump in rates at specific ν values as expected for a near-resonant transition. Furthermore, it was anticipated that for higher ν values, which do not satisfy the resonance condition, the rates should level again, but no further experiments have been performed to test this prediction.

B. Database of V-V and V/T-R rate coefficients

The quantum classical method in combination with the new PES gives excellent agreement (often within 25%) with the available experimental data for V-V and V-T/R scattering processes, as well as for the other measured quantities the potential was tested against. We, thus, used this combination to build a large dataset for V-V and V-T/R rate coefficients.

In order to gain a reasonable modeling of nonequilibrium systems, a large number of kinetic processes involving a variety of initially vibrationally excited states are, in fact, required for a wide temperature range. This makes the use of very accurate full quantum mechanical methods for the dynamics quite unpractical, particularly when heavy nuclei are involved. Furthermore, as mentioned in Sec. IV A, the calculation of accurate V-T/R rate coefficients needs very large initial separation distances to be considered, which makes them very time-consuming. This is why databases of V-T/R rate coefficients are usually not available in the literature. The quantum-classical method has shown to be as reliable as full quantum calculations and more effective than quasi classical trajectory methods to predict the matrix of inelastic rates in the whole temperature range.

In the present work, we consider vibrational quantum numbers up to 30. In fact, for very high vibrational excitation, the accuracy of Morse potential and Morse wavefunction used in the quantum classical treatment decreases. The same holds for the potential energy surface, which, as described above, is reliable up to $\nu = 25$. Furthermore, the reaction probability increases with vibrational excitation and neither the coupled state quantum classical methods nor the present PES can deal with reactive processes. However, we believe the above sources of inaccuracy to be negligible up to $\nu \leq 25$ and that they remain small up to $\nu = 30$ (although the data for the highest ν should be taken with more care). For even higher ν values, the present approach is still likely to provide a correct qualitative behavior, but quantitative accuracy would be diminished. Efforts are in progress to use a grid-based quantum classical method,⁷³ tailored to deal with reactivity, providing a more correct treatment of highly excited vibrational states.

We calculated V-V and V-T/R rate coefficients for single- and multi-quantum vibrational transitions by using the same specifications (number of coupled states and number of trajectories) described in Sec. IV A.

Numerical values of the rate constants at selected temperatures are listed in Tables S7-S13 of the [supplementary material](#). Here, we

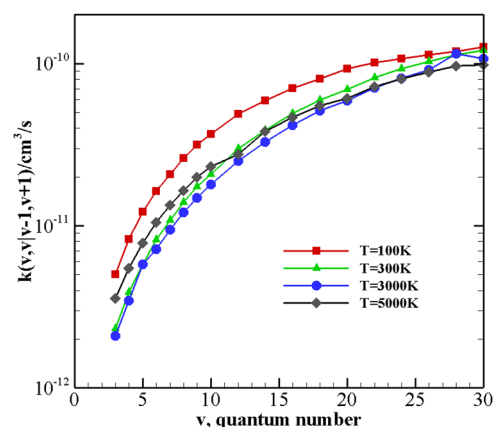


FIG. 7. V-V rate coefficients for $O_2(v) + O_2(v) \rightarrow O_2(v-1) + O_2(v+1)$ processes as a function of the vibrational quantum number ν at different temperature values.

report and discuss the behavior of the rates with temperature and/or with the vibrational quantum numbers.

Figure 7 shows the calculated V-V rate coefficients for the exothermic symmetric $O_2(v) + O_2(v) \rightarrow O_2(v-1) + O_2(v+1)$ processes as a function of the vibrational quantum number ν at 100 K, 300 K, 3000 K, and 5000 K. The numerical values are reported in Table S7. Rate coefficients increase with the quantum number ν at all temperatures as the process approaches the resonance (i.e., as ΔE approaches zero).

There is a significant anti-Arrhenius behavior of the rate coefficients, i.e., they decrease with the increase in the temperature in the low temperature regime for all the initial ν values; the extent of this phenomenon is such that the processes at 100 K are predicted to be the most efficient. This is also illustrated in Fig. S3, reporting

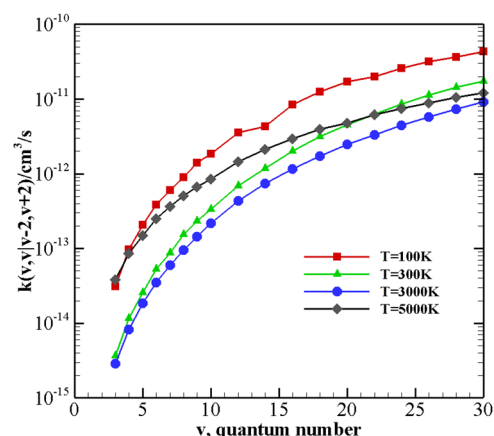


FIG. 8. V-V rate coefficients for $O_2(v) + O_2(v) \rightarrow O_2(v-2) + O_2(v+2)$ processes as a function of the vibrational quantum number ν at different temperature values.

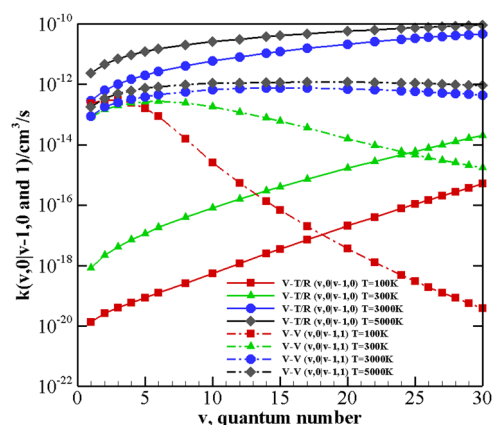


FIG. 9. V-V rate coefficients for the process $\text{O}_2(v) + \text{O}_2(0) \rightarrow \text{O}_2(v-1) + \text{O}_2(1)$ and V-T/R coefficients for $\text{O}_2(v) + \text{O}_2(0) \rightarrow \text{O}_2(v-1) + \text{O}_2(0)$ processes as a function of the vibrational quantum number v at different temperature values.

In k against $1/T$ for some selected initial v values at low T . Although this behavior is not unfrequent in V-V processes at very low T (as found both experimentally⁷⁴ and theoretically^{34,75} for collisions in molecular nitrogen), in the present case, it seems to hold up to $T \approx 1000$ K for all v investigated here, and only at higher temperature, the rate coefficients start to grow with temperature. Figure S3 shows that this is more relevant for relatively low v , which shows a nearly straight line with a significant positive slope, whereas for high v , the rate coefficients become almost independent of temperature (see also Table S7).

The same behavior is found for multiquantum symmetric processes:

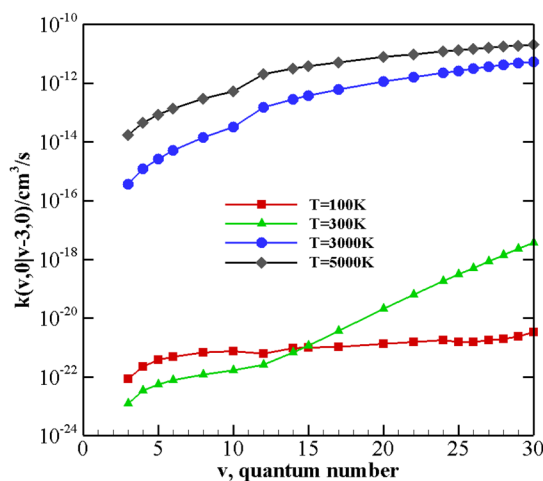
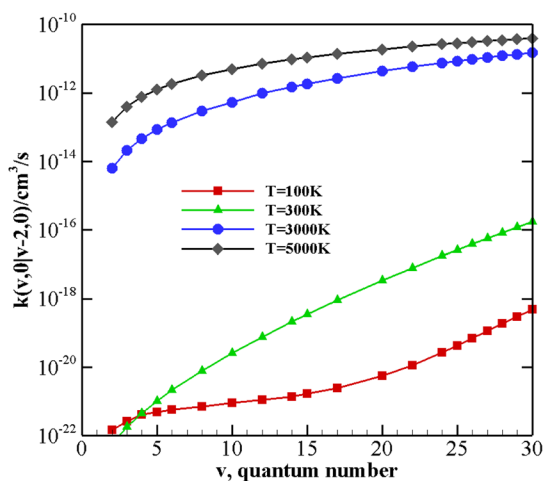


FIG. 10. V-T/R rate coefficients for $\text{O}_2(v) + \text{O}_2(0) \rightarrow \text{O}_2(v-w) + \text{O}_2(0)$ processes as a function of the vibrational quantum number v at different temperature values. $w = 2$ left panel, and $w = 3$ right panel.

$\text{O}_2(v) + \text{O}_2(v) \rightarrow \text{O}_2(v-w) + \text{O}_2(v+w)$, where $w = 2$ (Fig. 8) and 3 (Table S8). The efficiency in the symmetric exchange of vibrational quanta decreases as the exchanged number of quanta increases due to the energy mismatch (see Fig. S4 for $T = 1000$ K). The probability of exchanging a larger number of quanta becomes weaker, but it is still not negligible for higher vibrationally excited states.

V-V rate coefficients for the endothermic process $\text{O}_2(v) + \text{O}_2(0) \rightarrow \text{O}_2(v-1) + \text{O}_2(1)$ are reported in Fig. 9 as a function of v at different temperatures and in Table S9. They tend to strongly decrease with v at low temperature due to the larger energy mismatch, while they remain approximately constant at high temperature. Moreover, processes with small v values ($v \leq 5$) are nearly independent of temperature, whereas for larger v , the probability of vibrational energy exchange to excite the vibrational ground state is enhanced with temperature.

V-T/R rate coefficients were determined for processes where vibrational relaxation occurs due to the collision between O_2 in its vibrational ground state and a vibrationally excited molecule, with the loss of one, two, or more vibrational quanta (Tables S10–S12). The behavior of rate coefficients for V-T/R processes $\text{O}_2(v) + \text{O}_2(0) \rightarrow \text{O}_2(v-w) + \text{O}_2(0)$, with $w = 1, 2, 3$, as a function of the initial quantum number v at $T = 100$ K, 300 K, 3000 K, and 5000 K is reported in Figs. 9 and 10. The probability of losing vibrational energy decreases with the number of lost vibrational quanta w . In all cases, V-T/R rate coefficients show a stronger dependence on temperature than V-V ones so that they are very small in the low temperature regime. In fact, for low vibrational excited states, at $T \leq 300$ K, many of the V-T/R rate coefficients have an absolute value smaller than 10^{-20} cm^3/s , which is close to the numerical accuracy of the present method and their numerical value should be taken with some additional care. In such low T conditions, an anti-Arrhenius temperature behavior of the rate coefficients seems again to be present in the case of $w = 2$ and 3 for small v values. The turning point from an anti-Arrhenius to an Arrhenius behavior takes place at higher v values as w increases. For high temperature

values, the rate coefficients become much larger and the dependence on the ν value is smaller, although still slightly increasing with ν . In such a regime, the order of magnitude of the V-T/R rate coefficients is comparable or even larger than the corresponding symmetric V-V rate coefficients (Fig. 9), showing that the V-T/R transitions need to be included for a correct modeling of high temperature kinetics.

Vibrational relaxation upon collision between two equally vibrationally excited molecules $O_2(\nu) + O_2(\nu)$ was also considered (Table S13 and Fig. 11). Figure 11 shows the relative efficiency of the V-V and V-T/R processes corresponding to the same initial vibrationally excited states as a function of temperature for $\nu = 5, 10, 20$, and 30. A strong increase in the V-T/R rate coefficients with the temperature is again observed in all cases, whereas the V-V rate coefficients remain practically a plateau for the whole temperature

range, showing the above-mentioned anti-Arrhenius behavior with the temperature at low T. It is well known that under thermal and subthermal conditions, resonant and quasiresonant transitions are most effective, and the combined effect of long range intermolecular attraction and short range repulsive wall favors the trapping of the system in tight collision complexes and the coupling of the vibrational wavefunctions, favoring V-V processes. The large energy mismatch for V-T/R processes results in very low rate coefficients at low T. At high temperature, however, the V-T/R relaxation becomes comparable or faster with respect to V-V energy transfer, which remains the dominant process up to $T = 2000$ K. Temperatures above such a value, however, are of interest in plasma chemistry or in aerospace science, just to mention a few. The present study, thus, shows that the modeling of such conditions require the knowledge of V-T/R relaxation rates, besides the V-V ones.

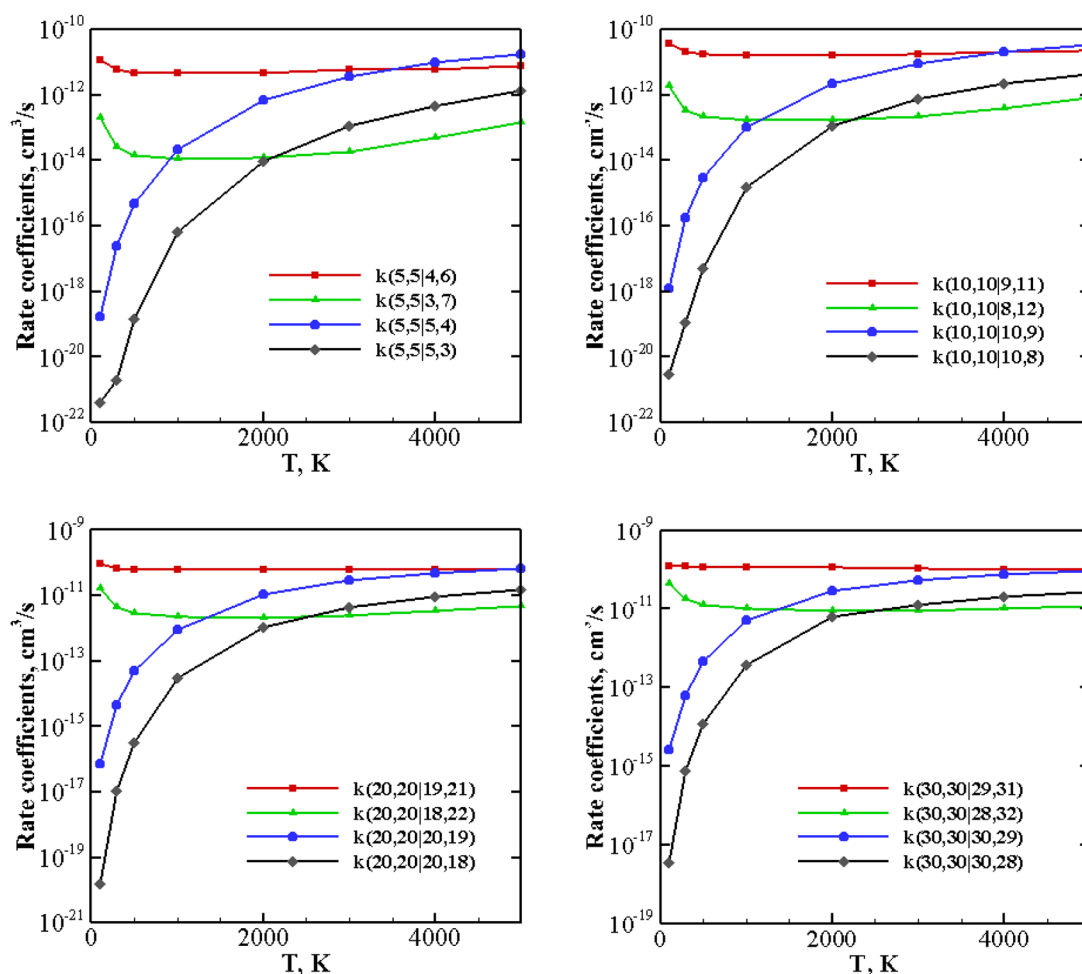


FIG. 11. V-T/R and V-V rate coefficients for some selected $O_2(\nu) + O_2(\nu)$ processes as a function of temperature for $\nu = 5, 10, 20$, and 30. The red line represents single-quantum V-V processes, the green line represents two-quantum V-V processes, the blue line represents single-quantum V-T processes, and the black line represents two-quantum V-T processes.

V. CONCLUSIONS

The present study provides an accurate description of the spin-averaged potential energy surface for $O_2(^3\Sigma_g^-)-O_2(^3\Sigma_g^-)$ interactions. The analytical potential energy surface is determined using a more flexible version of the improved Lennard-Jones method by adding the angular dependence to parameter β . Within this approach, the empirical parameters of the functional form of the potential are closely modulated by comparing the behavior of the PES against accurate high level *ab initio* calculations and assessing strength and anisotropy of the interaction against relevant experimental properties such as the quantum interference effects arising in scattering. This, in turn, produces very good agreement between properties calculated on the PES and the corresponding experimental values for a wealth of other data of various sources, such as the second virial coefficient, shear viscosity, thermal conductivity, and rate coefficients for vibrational exchange processes.

The limitations of the present model arise for important vibrational deformations of the diatoms (highly vibrationally excited states), for high temperature, where reactivity comes into play, and for high energy regimes, when vibronic energy exchange (V-E processes) should also be considered (e.g., involving the $a^1\Delta_g$ and $b^1\Sigma_g^+$ electronic states of O_2). However, this is meant to be a first step in the accurate description of the system: the above issues, together with additional effects (the differentiation between the spin multiplicities of O_2 and the inclusion of spin-orbit coupling), will be gradually considered and incorporated in future work. Nevertheless, we believe that it is important to start from a correct description of the long-medium range interaction. Such an approach is seldom used for the construction of PESs; nevertheless, there are, in fact, growing evidences that the final outcome of both inelastic and reactive collisional processes is determined by the formation of weakly bound adducts and of precursor states due to the orientation and alignment effects originating precisely in such a long distance region. The present methodology, thus, allows not only to correctly predict many valuable properties but also to project these relevant effects on the description of molecular deformations up to the opening of reactive channels and on the description of fine effects, which we are going to include as future steps.

In the present work, the PES was then used for the determination of a large database of V-V, as well as of V-T/R rate coefficients, whose calculation generally represents a computationally demanding task. The use of the quantum-classical method together with an efficient analytical formulation of the intermolecular potential makes it possible to perform such a task. The results show that V-V and V-T/R transitions of the title system are generally quite efficient in the temperature region considered here, the role played by V-T/R processes growing with temperature, until becoming, in some cases, the most probable events, suggesting that in the high temperature regime, they cannot be neglected for a proper modeling of non-equilibrium situations.

The approach described here for the construction of the non-reactive PES, based on a detailed accurate analytical model, whose parameters are fine-tuned within the range allowed by their physical meaning, is emerging as a highly efficient tool for the prediction of many properties determined by molecular interactions in a wide temperature range, and its applications to a number of atom-diatom and diatom-diatom systems are currently under study.

SUPPLEMENTARY MATERIAL

See the [supplementary material](#) for Figs. S1–S4 and Tables S1–S13 reporting single- and multi-quantum V–V and V–T/R rate coefficients in the temperature range 100 K–5000 K and the routine for the potential energy surface (in FORTRAN).

ACKNOWLEDGMENTS

This work was supported by the Strategic Priority Research Program of the Chinese Academy of Sciences (Grant No. XDA17030100) and the National Natural Science Foundation of China through Grant Nos. 11372325 and 91116013. M.B. acknowledges the FIS2017-84391-C2-2-P Spanish grant for fundings.

DATA AVAILABILITY

The data that support the findings of this study are available within the article and its [supplementary material](#).

REFERENCES

- H. Park and T. G. Slanger, " $O_2(X, \nu = 8-22)$ 300 K quenching rate coefficients for O_2 and N_2 , and $O_2(x)$ vibrational distribution from 248 nm O_3 photodissociation," *J. Chem. Phys.* **100**, 287–300 (1994).
- T. G. Slanger, "Energetic molecular oxygen in the atmosphere," *Science* **265**, 1817–1818 (1994).
- M. Klatt, I. W. M. Smith, R. P. Tuckett, and G. N. Ward, "State-specific rate constants for the relaxation of $O_2(X^3\Sigma_g^-, \nu = 8$ to 11) by collisions with NO_2 and O_2 ," *Chem. Phys. Lett.* **224**, 253–259 (1994).
- R. Hernández, R. Toumi, and D. C. Clary, "State-selected vibrational relaxation rates for highly vibrationally excited oxygen molecules," *J. Chem. Phys.* **102**, 9544–9556 (1995).
- D. A. Pejaković, Z. Campbell, K. S. Kalogerakis, R. A. Copeland, and T. G. Slanger, "Collisional relaxation of $O_2(X^3\Sigma_g^-, \nu = 1)$ and $O_2(a^1\Delta_g, \nu = 1)$ by atmospherically relevant species," *J. Chem. Phys.* **135**, 094309 (2011).
- V. Guerra and J. Loureiro, "Non-equilibrium coupled kinetics in stationary N_2-O_2 discharges," *J. Phys. D: Appl. Phys.* **28**, 1903 (1995).
- M. Capitelli, C. M. Ferreira, B. F. Gordiets, and A. I. Osipov, *Plasma Kinetics in Atmospheric Gases* (Springer Science & Business Media, 2013), Vol. 31.
- A. Annušová, D. Marinov, J. Booth, N. Sirse, M. L. da Silva, B. Lopez, and V. Guerra, "Kinetics of highly vibrationally excited $O_2(X)$ molecules in inductively-coupled oxygen plasmas," *Plasma Sources Sci. Technol.* **27**, 045006 (2018).
- D. A. Andrienko and I. D. Boyd, "Investigation of oxygen vibrational relaxation by quasi-classical trajectory method," *Chem. Phys.* **459**, 1–13 (2015).
- D. A. Andrienko and I. D. Boyd, "High fidelity modeling of thermal relaxation and dissociation of oxygen," *Phys. Fluids* **27**, 116101 (2015).
- Y. Paukku, K. R. Yang, Z. Varga, G. Song, J. D. Bender, and D. G. Truhlar, "Potential energy surfaces of quintet and singlet O_4 ," *J. Chem. Phys.* **147**, 034301 (2017).
- T. K. Mankodi, U. V. Bhandarkar, and B. P. Puranik, "Global potential energy surface of ground state singlet spin O_4 ," *J. Chem. Phys.* **148**, 074305 (2018).
- J. G. Kim, S. H. Kang, and S. H. Park, "Thermochemical nonequilibrium modeling of oxygen in hypersonic air flows," *Int. J. Heat Mass Transfer* **148**, 119059 (2020).
- J. Hao, J. Wang, and C. Lee, "State-specific simulation of oxygen vibrational excitation and dissociation behind a normal shock," *Chem. Phys. Lett.* **681**, 69–74 (2017).

- ¹⁵Q. Hong, X. Wang, Y. Hu, and Q. Sun, "Development of a stagnation streamline model for thermochemical nonequilibrium flow," *Phys. Fluids* **32**, 046102 (2020).
- ¹⁶Q. Hong, X. Wang, Y. Hu, X. Lin, and Q. Sun, "Rebuilding experimental nonequilibrium radiation in shock-heated Martian-like mixture flows using electronic state-to-state approach," *Int. J. Mod. Phys. B* **34**, 2040084 (2020).
- ¹⁷F. Esposito and M. Capitelli, "The relaxation of vibrationally excited O₂ molecules by atomic oxygen," *Chem. Phys. Lett.* **443**, 222–226 (2007).
- ¹⁸F. Esposito, I. Armenise, G. Capitta, and M. Capitelli, "O–O₂ state-to-state vibrational relaxation and dissociation rates based on quasiclassical calculations," *Chem. Phys.* **351**, 91–98 (2008).
- ¹⁹D. A. Andrienko, "The importance of O₃ excited potential energy surfaces in O₂–O high-temperature kinetics," *J. Chem. Phys.* **152**, 044305 (2020).
- ²⁰N. Balakrishnan, A. Dalgarno, and G. D. Billing, "Multi-quantum vibrational transitions in O₂($v \geq 25$) + O₂($v = 0$) collisions," *Chem. Phys. Lett.* **288**, 657–662 (1998).
- ²¹J. Campos-Martínez, E. Carmona-Novillo, J. Echave, M. I. Hernández, R. Hernández-Lamoneda, and J. Palma, "Jump in depletion rates of highly excited O₂: Reaction or enhanced vibrational relaxation?," *Chem. Phys. Lett.* **289**, 150–155 (1998).
- ²²C. Coletti and G. D. Billing, "Vibrational energy transfer in molecular oxygen collisions," *Chem. Phys. Lett.* **356**, 14–22 (2002).
- ²³V. Aquilanti, D. Ascenzi, M. Bartolomei, D. Cappelletti, S. Cavalli, M. de Castro Vitores, and F. Pirani, "Molecular beam scattering of aligned oxygen molecules. The nature of the bond in the O₂–O₂ dimer," *J. Am. Chem. Soc.* **121**, 10794–10802 (1999).
- ²⁴M. L. da Silva, J. Loureiro, and V. Guerra, "A multi-quantum dataset for vibrational excitation and dissociation in high-temperature O₂–O₂ collisions," *Chem. Phys. Lett.* **531**, 28–33 (2012).
- ²⁵M. Bartolomei, E. Carmona-Novillo, M. I. Hernández, J. Campos-Martínez, and R. Hernández-Lamoneda, "Accurate *ab initio* intermolecular potential energy surface for the quintet state of the O₂(³Σ_g[−])–O₂(³Σ_g[−]) dimer," *J. Chem. Phys.* **128**, 214304 (2008).
- ²⁶M. Bartolomei, E. Carmona-Novillo, M. I. Hernández, J. Campos-Martínez, and R. Hernández-Lamoneda, "Global *ab initio* potential energy surfaces for the O₂(³Σ_g[−]) + O₂(³Σ_g[−]) interaction," *J. Chem. Phys.* **133**, 124311 (2010).
- ²⁷Y. Paukku, Z. Varga, and D. G. Truhlar, "Potential energy surface of triplet O₄," *J. Chem. Phys.* **148**, 124314 (2018).
- ²⁸M. S. Grover, E. Torres, and T. E. Schwartztruber, "Direct molecular simulation of internal energy relaxation and dissociation in oxygen," *Phys. Fluids* **31**, 076107 (2019).
- ²⁹M. A. Valentin-Rodríguez, M. Bartolomei, M. I. Hernández, J. Campos-Martínez, and R. Hernández-Lamoneda, "An unrestricted approach for the accurate calculation of the interaction potentials of open-shell monomers: The case of O₂–O₂," *J. Chem. Phys.* **152**, 184304 (2020).
- ³⁰B. Bussery and P. E. S. Wormer, "A van der Waals intermolecular potential for (O₂)₂," *J. Chem. Phys.* **99**, 1230–1239 (1993).
- ³¹J. Li and H. Guo, "Permutationally invariant fitting of intermolecular potential energy surfaces: A case study of the Ne–C₂H₂ system," *J. Chem. Phys.* **143**, 214304 (2015).
- ³²Y. Liu, Y. Huang, J. Ma, and J. Li, "Classical trajectory study of collision energy transfer between Ne and C₂H₂ on a full dimensional accurate potential energy surface," *J. Phys. Chem. A* **122**, 1521–1530 (2018).
- ³³J. Li, Z. Varga, D. G. Truhlar, and H. Guo, "Many-body permutationally invariant polynomial neural network potential energy surface for N₄," *J. Chem. Theory Comput.* **16**, 4822–4832 (2020).
- ³⁴Q. Hong, Q. Sun, M. Bartolomei, F. Pirani, and C. Coletti, "Inelastic rate coefficients based on an improved potential energy surface for N₂ + N₂ collisions in a wide temperature range," *Phys. Chem. Chem. Phys.* **22**, 9375–9387 (2020).
- ³⁵D. Cappelletti, F. Pirani, B. Bussery-Honvault, L. Gomez, and M. Bartolomei, "A bond-bond description of the intermolecular interaction energy: The case of weakly bound N₂–H₂ and N₂–N₂ complexes," *Phys. Chem. Chem. Phys.* **10**, 4281–4293 (2008).
- ³⁶V. Aquilanti, D. Ascenzi, M. Bartolomei, D. Cappelletti, S. Cavalli, M. de Castro Vitores, and F. Pirani, "Quantum interference scattering of aligned molecules: Bonding in O₄ and role of spin coupling," *Phys. Rev. Lett.* **82**, 69–72 (1999).
- ³⁷G. Billing, "Rate constants and cross sections for vibrational transitions in atom-diatom and diatom-diatom collisions," *Comput. Phys. Commun.* **32**, 45–62 (1984).
- ³⁸G. Billing, "Rate constants for vibrational transitions in diatom-diatom collisions," *Comput. Phys. Commun.* **44**, 121–136 (1987).
- ³⁹D. Babikov and A. Semenov, "Recent advances in development and applications of the mixed quantum/classical theory for inelastic scattering," *J. Phys. Chem. A* **120**, 319–331 (2016).
- ⁴⁰G. Billing, "The semiclassical treatment of molecular roto-vibrational energy transfer," *Comput. Phys. Rep.* **1**, 237–296 (1984).
- ⁴¹R. Hamming, *Numerical Methods for Scientists and Engineers* (Dover Publications, New York, 1986).
- ⁴²G. D. Billing and L. Wang, "Semiclassical calculations of transport coefficients and rotational relaxation of nitrogen at high temperatures," *J. Phys. Chem.* **96**, 2572–2575 (1992).
- ⁴³C. S. Wang Chang, G. E. Uhlenbeck, and J. de Boer, *Studies in Statistical Mechanics* (North-Holland Publishing, 1964).
- ⁴⁴F. Pirani, S. Brizi, L. F. Roncaratti, P. Casavecchia, D. Cappelletti, and F. Vecchiocattivi, "Beyond the Lennard-Jones model: A simple and accurate potential function probed by high resolution scattering data useful for molecular dynamics simulations," *Phys. Chem. Chem. Phys.* **10**, 5489–5503 (2008).
- ⁴⁵G. Herzberg, *Spectra of Diatomic Molecules* (Van Nostrand Reinhold, New York, 1950).
- ⁴⁶F. Pirani, M. Albertí, A. Castro, M. M. Teixidor, and D. Cappelletti, "Atom-bond pairwise additive representation for intermolecular potential energy surfaces," *Chem. Phys. Lett.* **394**, 37–44 (2004).
- ⁴⁷C. Douketis, G. Scoles, S. Marchetti, M. Zen, and A. Thakkar, "Intermolecular forces via hybrid Hartree-Fock-SCF plus damped dispersion (HFD) energy calculations. An improved spherical model," *J. Chem. Phys.* **76**, 3057–3063 (1982).
- ⁴⁸R. Candori, F. Pirani, and F. Vecchiocattivi, "The N₂–Ar potential energy surface," *Chem. Phys. Lett.* **102**, 412–415 (1983).
- ⁴⁹M. Bartolomei, E. Carmona-Novillo, M. I. Hernández, J. Campos-Martínez, and R. Hernández-Lamoneda, "Long-range interaction for dimers of atmospheric interest: Dispersion, induction and electrostatic contributions for O₂–O₂, N₂–N₂ and O₂–N₂," *J. Comput. Chem.* **32**, 279–290 (2011).
- ⁵⁰E. García, A. Laganà, F. Pirani, M. Bartolomei, M. Cacciatore, and A. Kurnosov, "Enhanced flexibility of the O₂ + N₂ interaction and its effect on collisional vibrational energy exchange," *J. Phys. Chem. A* **120**, 5208–5219 (2016).
- ⁵¹D. E. Woon and T. H. Dunning, "Gaussian basis sets for use in correlated molecular calculations. V. Core-valence basis sets for boron through neon," *J. Chem. Phys.* **103**, 4572 (1995).
- ⁵²D. G. Truhlar, "Basis-set extrapolation," *Chem. Phys. Lett.* **294**, 45–48 (1998).
- ⁵³R. T. Pack, "Anisotropic potentials and the damping of rainbow and diffraction oscillations in differential cross sections," *Chem. Phys. Lett.* **55**, 197–201 (1978).
- ⁵⁴J. Dymond and E. Smith, *Virial Coefficients of Pure Gases and Mixtures. A Critical Compilation* (Clarendon, Oxford, 1980).
- ⁵⁵D. E. Gray, *American Institute of Physics Handbook* (McGraw-Hill, 1972).
- ⁵⁶G. P. Matthews, C. M. S. R. Thomas, A. N. Dufty, and E. B. Smith, "Viscosities of oxygen and air over a wide range of temperatures," *J. Chem. Soc., Faraday Trans.* **72**, 238–244 (1976).
- ⁵⁷A. A. Clifford, P. Gray, and A. C. Scott, "Viscosities of gaseous argon, oxygen and carbon monoxide between 273 and 1300 K," *J. Chem. Soc., Faraday Trans.* **71**, 875–882 (1975).
- ⁵⁸J. M. Hellemons, J. Kestin, and S. T. Ro, "The viscosity of oxygen and of some of its mixtures with other gases," *Physica* **65**, 362–375 (1973).
- ⁵⁹S. Ormonde, "Vibrational relaxation theories and measurements," *Rev. Mod. Phys.* **47**, 193–257 (1975).
- ⁶⁰G. D. Billing, "Semiclassical calculation of the rate constant for the process N₂($v = 1$) + N₂($v = 0$) → 2N₂($v = 0$) + 2330.7 cm^{−1} at low temperatures," *Chem. Phys. Lett.* **76**, 178–182 (1980).

- ⁶¹K. S. Kalogerakis, R. A. Copeland, and T. G. Slanger, "Vibrational energy transfer in $O_2(X^3\Sigma_g^-, \nu = 2,3) + O_2$ collisions at 330 K," *J. Chem. Phys.* **123**, 044309 (2005).
- ⁶²A. Tai, I. Adamovich, and W. R. Lempert, "Stimulated Raman scattering measurements of V-V transfer in oxygen," *Chem. Phys.* **323**, 532–544 (2006).
- ⁶³S. S. Watanabe, S. Y. S. Usuda, H. H. Fujii, H. H. Hatano, I. I. Tokue, and K. K. Yamasaki, "Vibrational relaxation of $O_2(X^3\Sigma_g^-, \nu = 9-13)$ by collisions with O_2 ," *Phys. Chem. Chem. Phys.* **9**, 4407 (2007).
- ⁶⁴S. Watanabe, H. Kohguchi, and K. Yamasaki, "Vibrational relaxation of $O_2(X^3\Sigma_g^-, \nu = 6-8)$ by collisions with $O_2(X^3\Sigma_g^-, \nu = 0)$: Solution of the problems in the integrated profiles method," *J. Phys. Chem. A* **116**, 7791–7796 (2012).
- ⁶⁵J. Price, J. Mack, C. Rogaski, and A. Wodtke, "Vibrational-state-specific self-relaxation rate constant. Measurements of highly vibrationally excited $O_2(\nu = 19-28)$," *Chem. Phys.* **175**, 83–98 (1993).
- ⁶⁶K. M. Hickson, P. Sharkey, I. W. M. Smith, A. C. Symonds, R. P. Tuckett, and G. N. Ward, "Formation and relaxation of $O_2(X^3\Sigma_g^-)$ in high vibrational levels (18–23) in the photolysis of O_3 at 266 nm," *J. Chem. Soc., Faraday Trans.* **94**, 533–540 (1998).
- ⁶⁷R. Hernández-Lamoneda, M. I. Hernández, E. Carmona-Novillo, J. Campos-Martínez, J. Echave, and D. Clary, "Theoretical evidence of the reaction $O_2(\nu) + O_2(\nu = 0) \rightarrow O_3 + O$," *Chem. Phys. Lett.* **276**, 152 (1997).
- ⁶⁸R. T. Jongma, S. Shi, and A. Wodtke, "Electronic nonadiabaticity in highly vibrationally excited $O_2(X^3\Sigma_g^-)$: Spin-orbit coupling between $(X^3\Sigma_g^-)$ and $(b^1\Sigma_g^+)$," *J. Chem. Phys.* **111**, 2588–2594 (1999).
- ⁶⁹R. T. Jongma and A. Wodtke, "Fast multiquantum vibrational relaxation of highly vibrationally excited O_2 ," *J. Chem. Phys.* **111**, 10957–10963 (1999).
- ⁷⁰F. Dayou, J. Campos-Martínez, M. I. Hernández, and R. Hernández-Lamoneda, "Spin-orbit coupling in $O_2(\nu) + O_2$ collisions: A new energy transfer mechanism," *J. Chem. Phys.* **120**, 10355–10358 (2004).
- ⁷¹F. Dayou, M. I. Hernández, J. Campos-Martínez, and R. Hernández-Lamoneda, "Spin-orbit coupling in $O_2(\nu) + O_2$ collisions. I. Electronic structure calculations on dimer states involving the $X^3\Sigma_g^-$, $a^1\Delta_g$, and $b^1\Sigma_g^+$ states of O_2 ," *J. Chem. Phys.* **123**, 074311–74323 (2005).
- ⁷²F. Dayou, M. I. Hernández, J. Campos-Martínez, and R. Hernández-Lamoneda, "Spin-orbit coupling in $O_2(\nu) + O_2$ collisions. II. Quantum scattering calculations on dimer states involving the $X^3\Sigma_g^-$, $a^1\Delta_g$, and $b^1\Sigma_g^+$ states of O_2 ," *J. Chem. Phys.* **126**, 194309 (2007).
- ⁷³C. Martí, L. Pacifici, A. Laganà, and C. Coletti, "A quantum-classical study of the OH + H_2 reactive and inelastic collisions," *Chem. Phys. Lett.* **674**, 103–108 (2017).
- ⁷⁴R. Z. Martínez and D. Bermejo, "Experimental determination of the rate of V-V collisional relaxation in $^{14}N_2$ in its ground ($X^1\Sigma_g^+$) electronic state between 77 and 300 K," *Phys. Chem. Chem. Phys.* **17**, 12661–12672 (2015).
- ⁷⁵A. Kurnosov, M. Cacciatore, A. Laganà, F. Pirani, M. Bartolomei, and E. Garcia, "The effect of the intermolecular potential formulation on the state-selected energy exchange rate coefficients in N_2 - N_2 collisions," *J. Comput. Chem.* **35**, 722–736 (2014).